LES of spray and combustion in an internal combustion engine

By D. Kah, V. Mittal, Shashank AND H. Pitsch

1. Motivation and objectives

With the ever rising need for better fuel efficiency and lower emissions, the development of better engine technology is essential. Different strategies are being considered to increase engine efficiency, such as direct injection or downsizing. Certain regimes are clearly identified as optimal for certain range of loads. For gasoline engines, the Homogeneous Charge Compression Ignition (HCCI) concept produces very low pollutants for low loads. At higher loads, however, the fast pressure rise can lead to engine damage and high noise levels. The Spark Ignition (SI) regime is the best suited for those cases. But pollutants emission is very high. In order to combine the best of the two regimes, a strategy consists in developing a hybrid SI and HCCI engine, functioning in HCCI regime at low loads, and SI regime at high loads. As the complexity of these strategies increases, the issue of monitoring and controlling the regime transition becomes a challenge. Therefore, numerical simulation is becoming an increasingly necessary complement to experiments. In order to make a significant impact simulation needs to reach two purposes. First, in the turbulent reactive flows occurring in Internal Combustion (IC) engines, the mixing of the reactants enabling the chemical reaction happens at the turbulence scales. Capturing this process accurately is essential to predict fuel and air distribution in the cylinder. Secondly, describing the dynamics of the transition between the two modes requires to capture cycle-to-cycle variations. With Reynolds Averaged Naviers-Stokes (RANS) approaches, all turbulence scales are modeled. Hence it does not accurately predict turbulent mixing. Besides RANS methods loose information about various unsteady processes, making it unable to predict cycle-to-cycle variations. With the increase in computational ressources, Large Eddy Simulations (LES) can now be considered. In contrast to Reynolds Averaged Navier-Stokes (RANS), LES can capture cyclic variations, which is essential when transitioning from one regime to another. Turbulence mixing is also better captured. Simulation of IC engines requires to solve for multi-physics processes: gas exchange, spray injection and combustion. This work investigates the spray modeling in this context. A Lagrangian method is used for this purpose. Even though spray models already exist in RANS, they cannot be used as are. Indeed, spray evaporation is a key process conditioning the structure of the mixture. Many models are proposed in the literature, so the first step is to determine the evaporation model best suited to our case. Spray models contain several phenomenological parameters that need to be calibrate for our case of interest. Once validated, the spray model needs to be set up for realistic engine computations. The test case chosen is an HCCI case. The capacity of the mixture resulting to auto-ignite is the validation criterion investigated here. Combustion is solved for with the RIF model (Pitsch *et al.* 1996; Barths *et al.* 1999; Mittal *et al.* 2012).

The remainder is organized as follows. In Section 2, the gas phase resolution and the combustion model are briefly explained. Then the spray model is explained with a

synthetic description of the most important modeling choices. Section 3 presents first the validation strategy, as well as some sensitivity results to the parameters of the spray model. Then first results of fuel injection in an LES framework in non-reactive and reactive configurations are presented. Finally a summary of the work and perspectives are presented in conclusion.

2. Modeling and numerical framework

This section presents the essential aspects of the modeling framework as well as the numerical methods.

2.1. *Gas phase*

The Navier-Stokes equations used to describe the flow field are:

$$\begin{aligned}
\partial_t \rho + \partial_{x_j}(\rho u_j) &= S_m, \\
\partial_t(\rho u_i) + \partial_{x_j}(\rho u_j u_i) &= -\partial_x P + \partial_{x_j}\tau_{ij} + S_{mom,i}, \\
\partial_t(\rho Y_k) + \partial_{x_j}(\rho u_j Y_k) + \partial_{x_j}(\rho V_{k,j}) &= \dot{\omega}_k + S_{m,k}, \\
\partial_t(\rho e) + \partial_{x_j}(\rho u_j e) + P\partial_{x_j}(u_j) &= \tau_{ij}\partial_{x_j}(u_j) + \partial_{x_j}(\lambda \partial_{x_j} T) \\
&\quad -\partial_{x_j}(q_{FLUX}) - \dot{q}_{\Delta h} + S_{en}, \\
q_{FLUX} &= \rho \sum_{k=1}^{N} h_k Y_k V_{k,j}, \\
h &= \int_{T_0}^{T} C_p \, \mathrm{d}T + \sum_{k=1}^{N} \Delta h^0_{f,k} Y_k,
\end{aligned} \tag{2.1}$$

where P denotes the pressure and τ_{ij} is the viscous stress tensor defined by the Boussinesq approximation. The quantity Y_k denotes the mass fraction of the k^{th} species and $V_{k,j}$ is its diffusion velocity. The scalar denotes the gas internal energy, λ the thermal conductivity, T the temperature. The quantity C_p is the mixture averaged specific heat capacity at constant pressure over N species, q_{FLUX} the enthalpy flux, h represents the sum of sensible and chemical enthalpies, and $\Delta h^0_{f,k}$ is the heat of formation of species k. Finally, q_{FLUX} denotes the heat losses of the system.

A Fick law is used to compute the diffusion velocity of species k: $V_{k,j} = -D_k \partial_{x_j}(Y_k)$. In the general case of the diffusitivity coefficient being not equal, i.e., $D_k \neq D$, the global mass is not conserved through the Fick law. Therefore, a correction velocity $V_{c,j}$ is introduced to ensure that the model for the diffusion velocity does not introduce a net flux (Poinsot & Veynante 2005), leading to $V_{k,j} = -D_k \partial_{x_j}(Y_k) + V_{c,j}$. The terms $S_m, S_{m,k}, S_{mom,i}, S_{en}$ denote the source terms from the spray. They are defined in Section 2.2.

The dynamic system for the gas is presented in the general case of a compressible flow, i.e., an explicit relationship is considered between the density, the pressure and the temperature. If this approach is the most general, it may lead to unnecessary large computational times if the hydrodynamic velocity of the system is very small compared to the speed of sound. In this context, the pressure term can be developed in a series expansion in terms of the Mach number. It turns out that the gradient of the thermodynamic pressure is the only term of order zero in the moment equation, leading to the fact that, in the limit of small Mach numbers, it is spatially uniform. The pressure term

of second order in Mach number remains in the momentum equation. This term, called the hydrodynamic pressure, is a Lagrange multiplier computed in order to satisfy the continuity equation (Muller 1998). This Low-Mach approache significantly reduces the constrain on the time-step.

Given our target computational domain and the Reynolds numbers involved, a Direct Numerical Simulation, i.e., resolving the flow up to the Kolmogorov scale, would require a prohibitive cost. On the other hand, a RANS approach would provide only ensemble average information. This is not acceptable for the two reasons mentioned in the introduction. Therefore an LES framework is considered, i.e., a low-pass filter is applied to the equations instead of ensemble averaging. The explanation of the filter and the derivation of the equations can be found in (Poinsot & Veynante 2005). Then the dynamics of filtered quantities are solved. But their dynamics are impacted by sub-grid scale terms that appear throughout the filtering process: Reynolds stress, unresolved species and energy fluxes. Different models to close these terms exist in the literature (Smagorinsky 1963; Germano *et al.* 1991; Meneveau & Katz 2000). In this study, the dynamic Smagorinsky model (Germano *et al.* 1991) is used where the value of the constant is calculated locally by applying test filters and using knowledge about the energy cascade. A weighted averaging is performed backwards in time over Lagrangian trajectories of fluid particles (Meneveau *et al.* 1996).

In the context of IC Engines simulation, the computational geometry varies due to the piston movement. The strategy adopted in this work is to consider an Arbitrary Lagrangien Eulerian (ALE) formalism (Donea *et al.* 2004). The ALE formalism consists in writing the dynamic equation system in the grid reference frame. The complete derivation of the Navier-Stokes equation system in the ALE formalism can be found in (Kah 2010).

The reactive flow modeling is based on the flamelet assumption, implying that the configuration studied in this work lies in the limit of high Damkohler numbers. This means that the chemistry time scale is very fast compared to turbulence. Therefore, locally and as far chemistry is solved, the mixed flow has a laminar counter-flow flame structure. Since a non premixed case is studied, quantities that are linear combination of species and/or temperature and are constant through the chemical reaction can be derived from system (2.1): they are called mixture fractions. In the following we assume that one mixture fraction can characterize the flame structure. The flamelet equation system, first derived by Peters (1984) consists in writing equations on species and temperature in a set of coordinates that explicitly decouples the two processes, by isolating the mixture fraction Z as an independent variable.
Moreover, a combustion model is intrinsically linked to the regime it is supposed to describe. In HCCI settings, as the mixture is expected to be rather homogeneous, the auto-ignition regime is predominant. In this context, the unsteady combustion process has a strong dependence on the overall pressure which can vary significantly in the engine. Therefore, an interactive flamelet method is used to compute chemistry on the fly.
In an LES framework (this can also be applied to RANS) a sub-grid representation of the mixture fraction field is assessed by a probability density function (PDF) with a presumed profile constructed from the moment information of Z in the cell. The resulting species distributions in the mixture fraction co-ordinate are then convoluted with this PDF. This results in mean species mass fractions at each cell location. This procedure is explained in (Doran 2011). The corresponding model is called Representative Interactive Flamelet (RIF) (Pitsch *et al.* 1996; Barths *et al.* 1999; Mittal *et al.* 2012). The one-dimension RIF equation system writes:

$$\begin{aligned} \rho\partial_t h &= \frac{\rho\chi_Z}{2}\left(\frac{\partial^2 h}{\partial Z^2}\right) + dP/dt, \\ \rho\partial_t Y_k &= \frac{\rho\chi_Z}{2}\left(\frac{\partial^2 h}{\partial Z^2}\right) + \dot{\omega}_k, \end{aligned} \tag{2.2}$$

where χ_Z is the scalar dissipation rate associated to the mixture fraction. The RIF equations are presented here in one dimension for the sake of simplicity. We refer to (Mittal *et al.* 2012) for its extension to two-dimensions.

2.2. *Spray*

A Lagrangian method is considered to solve for the spray dynamics. This method, the Stochastic Parcel (SP) as used in (O'Rourke 1981), belongs to the family of statistical models. Many different models exist to describe Lagrangian spray dynamics. In the vast majority of cases, the equations that are solved to describe the drop position $x_{d,j}$, velocity $u_{d,j}$, temperature T_d, and mass m_d formally read

$$\begin{aligned} dx_{d,j}/dt &= u_{d,j} &&, \\ du_{d,j}/dt &= \dot{u}_{d,j} &&= \frac{\alpha}{\tau_d}(u_j - u_{d,j}), \\ dT_d/dt &= \dot{e}_d/C_L &&= \frac{\beta\bar{C_p}}{\tau_d}(T - \tau_d) + \frac{\dot{m}_d L_v}{m_d C_L}, \\ dm_d/dt &= \dot{m}_d &&= -\theta ln(1 + B_M), \end{aligned} \tag{2.3}$$

where L_v is the latent heat of evaporation, and C_L the specific heat of the droplet. The terms α, β, θ are function of the non-dimension numbers of the problem: relative Reynolds numbers, numbers relative to diffusion and transfer of mass and temperature).Various correlations are found in the literature. We use the expressions presented in (Shashank *et al.* 2011). System (2.4) describes gas-spray interaction through drag, heat transfer and evaporation. The source terms from the particles to the gas write:

$$\begin{aligned} S_m &= \sum_{p=1}^{N} \frac{n_p(\dot{m}_d)_p}{\mathcal{V}}, \\ S_{m,k} &= \sum_{p=1}^{N} \frac{n_p(\dot{m}_d\delta(k-f))_p}{\mathcal{V}}, \\ S_{mom,i} &= \sum_{p=1}^{N} \frac{n_p(\dot{u}_{d,i} + \dot{m}_d u_{d,i})_p}{\mathcal{V}}, \\ S_{en} &= \sum_{p=1}^{N} \frac{n_p(\dot{e}_d + \dot{m}_d C_L T_d)_p}{\mathcal{V}}, \end{aligned} \tag{2.4}$$

where p is the parcel index, and n_p is the number of physical particles per parcel, and $\mathcal{V}$ a characteristic elementary volume (taken as the computational cell volume in simulation as done in (Miller & Bellan 1999)). The Dirac symbol $\delta(k-f)$ means that the mass source is considered only if the species k is the evaporated fuel f. The purpose of this section is to briefly discussed the explicitly stated coefficients as their expressions are consequences of assumptions made for to solve system (2.2). The retained expressions are based on a sensitivity studied done in (Shashank *et al.* 2011) that highlights the set of assumptions that leads to the best comparison with experiment of an evaporating spray.

Let us first remark that only equilibrium models are considered. That is, the relationship between mole fraction and partial pressure is given by the Henry law: $Y_{d,s} =$

$P_{sat}(T_{d,s})/P$, where $Y_{d,s}$ denotes the fuel mass fraction at the droplet surface and P_{sat} the saturation pressure at temperature $T_{d,s}$ at the droplet surface. The first choice to make is to express the representative quantities of the surrounding gas, the heat capacity $\bar{C_p}$ and the viscosity μ_r that appear in the characteristic response time of the droplet $\tau_d = \frac{\rho_d d_d^2}{18\mu_r}$, where ρ_d is the drop density, and d_d its diameter. Considering $\bar{C_p}$, it is written using a standard mass weighting (Miller & Bellan 1999):

$$C_p = Y_{ref} C_{p,f} + (1 - Y_{ref}) C_{p,g}, \tag{2.5}$$

where $C_{p,f}$ is the specific heat of pure fuel and $C_{p,g}$ the specific heat of the ambient gas. Different values of Y_{ref} are considered in the literature, and the one that is retained in this work is given by the 1/3 rule: $Y_{ref} = 2/3Y_{d,s} + 1/3Y_f$, where Y_f is the fuel mass fraction in the ambient gas. The viscosity μ_r is also expressed with a 1/3 rule. The reference temperature T_{ref} at which $C_{p,f}$ and μ_r are computed is also expressed with a 1/3 rule.

The second choice concerns the surface temperature definition. The Henry law links $Y_{d,s}$ and $T_{d,s}$. Another relationship is given by an equation verified by the Spalding numbers in mass and temperature B_M and B_T. The general equation (Sazhin 2006) is written:

$$(1 + B_M)^{C_{p,f}/(C_{p,g} Le)} = B_T, \tag{2.6}$$

where Le is the Lewis number of the ambient gas. Some models solve the system made of the two previous equations, and unknows $Y_{d,s}$ and $T_{d,s}$. Others assume $Le = 1$, leading to an easier system to solve. Finally, some models directly assume $T_{d,s} = T_d$. Despite its simplicity, this last choice is recommended by (Shashank *et al.* 2011). The last choice concerns the expression of the function f in $Y_{d,s} = P_{sat}(T_{d,s})/P$. The Clapeyron relation is clearly shown in (Shashank *et al.* 2011) to be accurate only for pressures close to the atmospheric pressure. If the difference becomes too important, $P_{sat}(T_{d,s})$ must be derived from the Gibbs free energy equation of the species.

Given the potential high value of the Weber number, secondary break-up modeling is also considered in this work. As suggested in (Baumgarten 2006), a coupled Rayleigh-Taylor and Kelvin-Helmholtz model is considered. A criterion based on the distance to the injector set the model used for a given particle. The explanation of these models is beyond the scope of this paper. However it is very important to note that these models contain certain adjustable parameters according to the surrounding flows. The Rayleigh-Taylor model describes the burst of a mother droplet through differential acceleration with the gas. Children droplets have the same diameter, given by $\Gamma = C_3 2\pi \sqrt{\frac{3\sigma}{a(\rho_l - \rho_g)}}$ proportional to the wavelength of the instability, where σ is the surface tension. The adjustable parameter C_3 includes unknown effects of initial conditions like turbulence and cavitation inside the injector nozzle. It ranges from 1 to 5.33. Increasing its value amounts to reduce break-up, and then turbulence. The Kelvin-Helmholtz model accounts for surface waves that are sheared off the parent drop; the drop's radius varies continuously according to a relaxation equation $dr/dt = -\frac{r - r_{new}}{\tau_b}$. The value of r_{new} follows an algebraic relationship, but the characteristic time is written as $\tau_{bu} = 3.788 B_1 \frac{r}{\Gamma\Omega}$, where Ω is the fastest growth rate of the instability (Baumgarten 2006). Values between $B_1 = 1.73$ and $B_1 = 60$ are proposed in the literature. A higher value of B_1 leads to a reduced break-up, while a smaller value on the other hand results in increased spray

disintegration, faster fuel-air mixing and reduced penetration.

Despite the absence of any explicit LES model for the spray (the gas quantities in system (2.4) are the filtered quantities from system (2.1)), the effect of turbulence is taken into account in the parameters C_3 and B_1.

2.3. *Numerical framework*

The simulation set-up is structured and the grid is cartesian (we refer to (Mittal 2012) for a discussion on this choice). Spatial resolution is performed using a high-order accurate finite difference code, with a WENO 3 scheme in order to ensure boundedness of the scalars, important for reactive flows. A staggered representation is used where the velocity is defined at the cell face, while the scalars are located at the cell center.

In the Low-Mach flow solver, time integration is done using a second order semi-implicit Crank-Nicolson scheme. The Poisson system verified by the hydrodynamic pressure to satisfy the continuity equation is solved using the HYPRE library. For compressible flows, time integration is done with a second order, 5-stage explicit Runge-Kutta scheme (Stanescu & Habashi 1998). It allows a certain relaxation of the CFL condition as the stability limit is 3.52.

The dynamic Ordinary Differential Equation system for the spray is time-resolved using a second order Runge-Kutta scheme.

For the other aspects of the numerical architecture such as boundary conditions and object definition and movement, the reader is refered to (Mittal 2012).

3. Results

This section presents two types of results. First, a quantitative validation of the spray model and parameters in the LES context is presented. This validated spray model is then considered in the context of the computation of an HCCI engine cycle, and the second section presents first results of auto-ignition.

3.1. *Spray validation in a bomb chamber case*

As mentioned in Section 2.2, the spray model contains some parameters that need to be adjusted to the considered case. For the sake of efficiency, the number of studied parameters is limited to the three most relevant: the two parameters involved in the break-up and $\bar{d}$, the mean diameter of the injected distribution. The domain considered for this case is a simple cubic box of size 0.15 m. The fuel considered is ethanol, in order to compare with experiment results, and the ambient gas phase is nitrogen. For the computation, the thermodynamic quantities for ethanol were derived from its Gibbs free energy (Dillon & Penoncello 2004). The computation is conducted using a Low-Mach solver.

The case consists in spray injection in the box filled with steady gas. The spray size distribution follows the distribution proposed by (Dumouchel 2009):

$$f(d) = q \frac{\left(\frac{\alpha}{q}\right)^{\alpha/q}}{\Gamma\left(\frac{\alpha}{q}\right)} \frac{d^{\alpha-1}}{\bar{d}^{\alpha}} \exp\left(-\frac{\alpha}{q}\left(\frac{d}{\bar{d}}\right)^{q}\right), \tag{3.1}$$

where α and q are two parameters that control the profile of the distribution. They were set up by a previous computation performed at the Robert Bosch Corporation

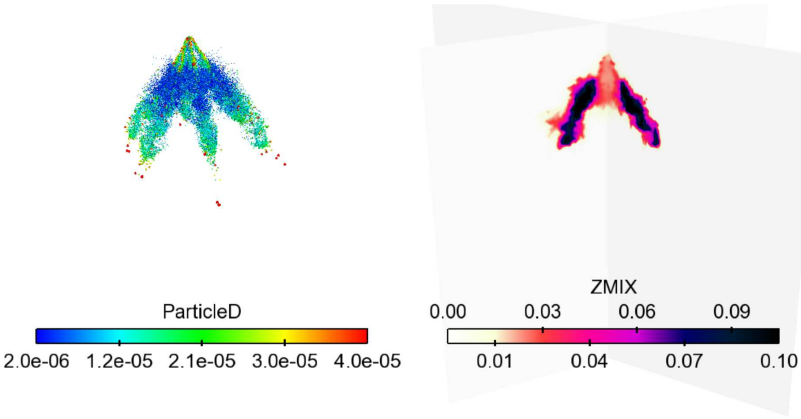

FIGURE 1. Spray particles and the mixture fraction at the start of injection.

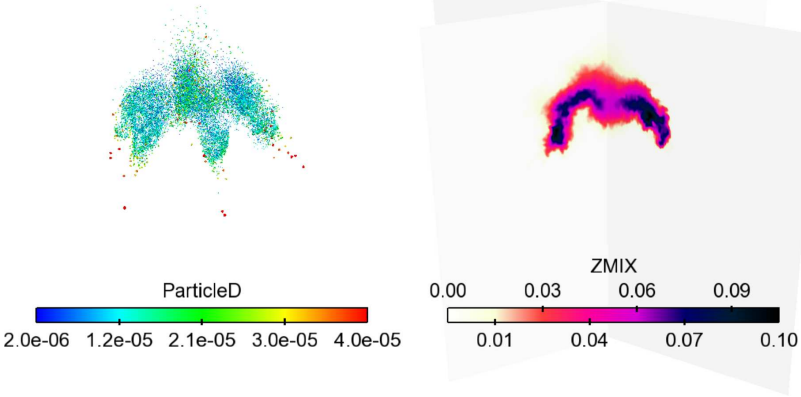

FIGURE 2. Spray particles and the mixture fraction at the end of injection.

and the same value is taken here ($\alpha = 3, q = 1.5$). During injection, numerical parcels are injected following a trapezoidal profile. Each parcel contains an integer number of physical particles. The size of each injected parcel is computed using a rejection method (de Chaisemartin 2009). The mass flow rate is read from the input. This quantity defines the number of injected parcels. The droplet velocity is computed through a Eulerian analogy with a continuous media stating that $\dot{m} = \rho S u$ where S is the given effective injector surface. A six-hole injector has been computed, defining the location, velocity and direction of injection in order to respect the experimental setup. The chamber is initiated with a temperature of $700K$, and droplets are injected with a temperature of $300K$.

Since the droplets are injected with a high velocity (over $100m/s$) a high level of turbulence is expected, therefore the lower range values of the break-up coefficients are considered. Snapshots of the particles and the mixture fraction field, representing the evaporated fuel fraction in gas, are represented in Figure 1 and Figure 2. The 3-D field of mixture fraction is represented through two orthogonal plans. The break-up is very intense in the region of high concentration of small particles.

Tests have been performed varying the values of the parameters, and the curves displayed in Figure 3 to Figure 6 are the penetration length, defined as the distance between

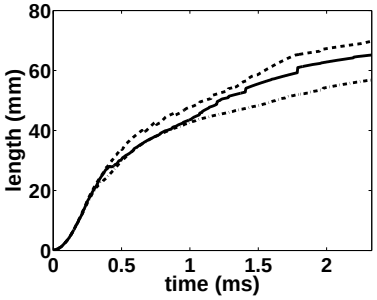

FIGURE 3. Injection with increasing $\bar{d}$: $15\mu m$ ($\cdot$ - $\cdot$), $16\mu m$ (—), $18\mu m$ (- -).

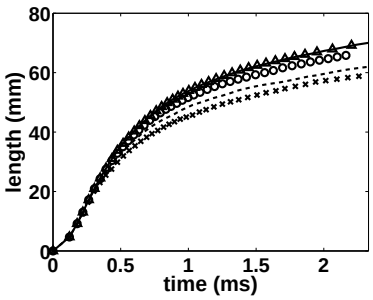

FIGURE 4. Injection with increasing B_1: 10 ($\times\times$), 12 (- -), 14 ($\circ\circ$), 15 (—), 20 ($\triangle$ $\triangle$).

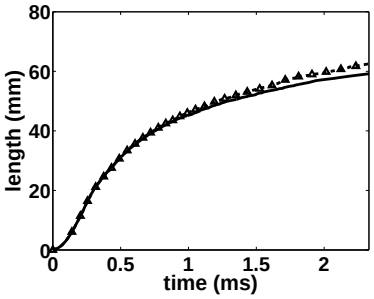

FIGURE 5. Injection with increasing C_3: 1 (—), 2 (- -), 3 ($\triangle$ $\triangle$).

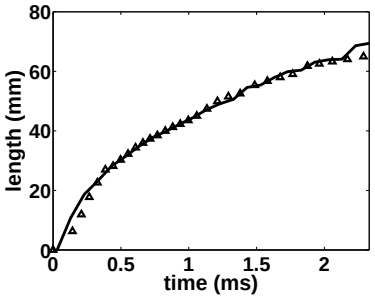

FIGURE 6. Comparison simulation ($\triangle$ $\triangle$) and experience (—).

the injector and the particle that went further than 99% of the particle population. First, in Figure 3, the mean injected diameter varies from $15\,\mu m$ to $18\,\mu m$ and as expected the biggest the droplets are, the further they penetrate in the chamber. In the next test, Figure 4, the Kelvin-Helmholtz coefficient B_1 varies from 10 to 25, with $\bar{d} = 15\,\mu m$ and $C_3 = 3$. Here again, as predicted, the lower B_1, the lower the penetration length. Interestingly, the range where B_1 affects the penetration length profile is below 20 or even 15. Varying the Rayleigh-Taylor coefficient has a little impact, as seen on Figure 5. This effect comes from the fact that the KH model is called after the RT. Smaller droplets created by the RT model will lead the KH model to decrease the break-up intensity, whereas bigger droplets occuring after the RT step will lead the KH model to increase the break-up intensity. In that sense the KH model can be thought of as a relaxation towards a certain size. The last result displayed in Figure 6, presents a comparison with the converged set of parameters and the experimental results. This excellent level of comparison validates our approach. The set of parameter is $\bar{d} = 16\,\mu m, B_1 = 8, C_3 = 2$.

3.2. *Engine case*

In this section, the spray numerical framework is adapted in the context of a gasoline engine computation in HCCI regime. The selected regime considers a compression ratio of 11 and 1800 revolutions per minute. The compression ratio is the volume ratio between the volume at Bottom Dead Center and Top Dead Center. In this realistic computation case, gas intake and exhaust are described through valve motion, as well as piston motion. The motion of the piston, intake valve, and exhaust valve is prescribed using the profiles shown in Figure 7. The handling of these objects motion is explained in (Mittal

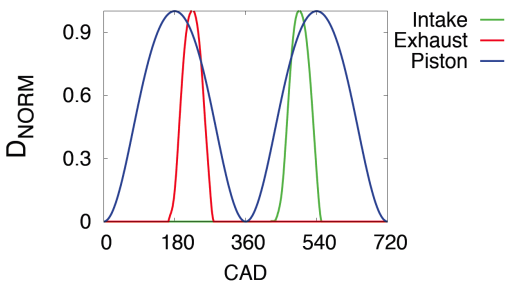

FIGURE 7. Displacement profiles of the piston, intake valve, and exhaust valve against Crank Angle in the engine computation. Source: (Mittal 2012).

2012). During the intake process, the gas velocity is such that a Low-Mach assumption is incorrect. Therefore a compressible model is considered. The computation starts at 360 Crank Angle (CAD) when the piston is at the TDC location, and injection occurs in the immediate aftermath, with the liquid mass rate following a trapezoidal profile as before. The initial conditions for the gas are $P = 16.5$ bars and $T = 1250\,\mathrm{K}$. The prescription of consistent boundary conditions in the manifolds is done following the NSCBC methods (Mittal 2012).

Non-reactive gas exchange simulations have already been performed by (Mittal 2012). The challenge addressed here is to ensure stability adding spray injection. The numerical tools validated in the previous case are used, but several new aspects needed to be investigated. First, the consistency of the two-way coupling terms from the spray to the gas has been enforced in a compressible framework for the gas. The fact that different scalars are transported whether the gas solver is compressible or Low-Mach is taken into account in the coupling procedure. Besides, some adjustments have been made to the evaporation model in order to cope with high gas temperatures that would lead to a temperature over the critical point of the liquid. Furthermore, scalar fluxes due to mesh movement have been adjusted so that discrete maximum principle is enforced for concerned scalars like mixture fraction. Finally the spray-wall interaction algorithm has been completed considering a new case that may occur when the wall is not aligned with a canonical direction. The fuel is considered to be iso-octane which is considered to have properties similiar enough to gasoline for our purposes. Its thermodynamic properties are read from NIST tables (http://webbook.nist.gov/chemistry/ 2011). For verification purposes of the code stability of this case, a computation on a relatively coarse mesh $102 \times 66 \times 82$ is considered.

The computation is run in two steps. The first one, from 360 CAD to 660 CAD solves for gas exchange and injection in a non-reactive framework. Then at 660 CAD, 60 CAD before the piston reaches the TDC location, and when ignition is about to be expected, the computation is run with the flow solver coupled to the RIF solver.

Results of the non-reactive case are shown in Figure 8 and Figure 9 where the spray particles are represented at the right side and the mixture fraction field between fuel and ambient gas is represented in the left side on two orthogonal planes. The mixture fraction field is linked to the evaporated fuel, and the figures show that it is mixed in the domain as time goes on. They also demonstrated the good qualitative behavior of the numerics, as the zones of high mixture fraction corresponds to zones where the particle stream has long residence time.

In the reactive case, species and temperature are solved according to system (2.2)

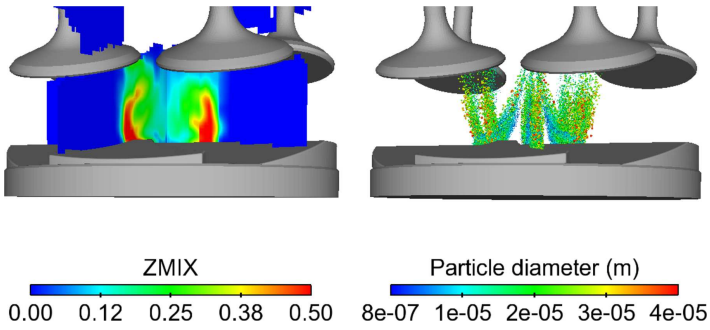

FIGURE 8. Spray injection in engine at 400 CAD. left:mixture fraction; right:spray.

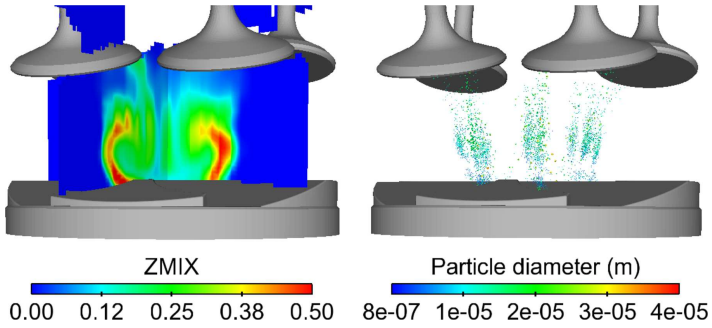

FIGURE 9. Spray injection in engine at 423 CAD. left:mixture fraction; right:spray.

where one representative variable, the mixture fraction, is considered. The initial fields are read from the result of the non-reactive computation. Figures (10 and 11) show that auto-ignition occurs. This result, although purely qualitative, validates the numerical architecture and paves the way to further developments and computations.

4. Conclusion and perspectives

This paper presents a contribution to build a modeling and numerical framework for LES computations of IC engines including multi-physic aspects such as gas exchange, spray injection and combustion. This work focuses on the integration of a spray solver in this architecture. It consists of the implementation of the model presented in (Shashank *et al.* 2011) in the LES code CIAO. The model parameterization in an LES framework has then been preliminary validated in the context of injection of ethanol in a bomb chamber containing nitrogen. This spray solver has then been set up to the overall engine computation framework. First validation test cases in HCCI regime have demonstrated the robustness of the solver. In particular, the field of the mixture fraction between fuel and ambient gas has lead to auto-ignition. These promising results pave the way for computations in a fine mesh where the biggest turbulence structures can be resolved. Besides, the spray-wall interaction which is a simple reflexion as seen in Figure 8 should be improved by implementing a wall-jet model, more representative of the reality. Then comparison with experimental data will assess the relevance of our approach. Moreover, studied carried out have shown that an intermediate mode, Spark Assisted Compression

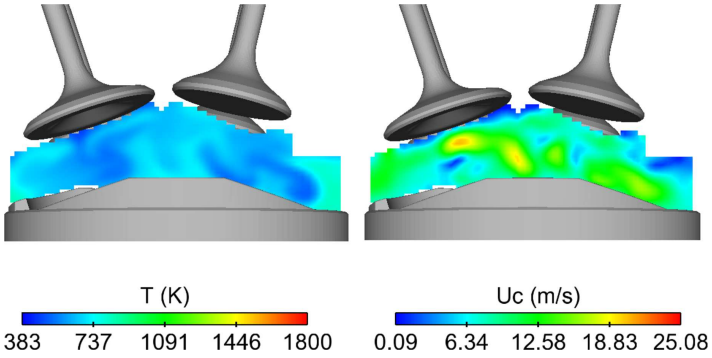

FIGURE 10. Reactive case at 685 CAD. left: temperature; right: velocity.

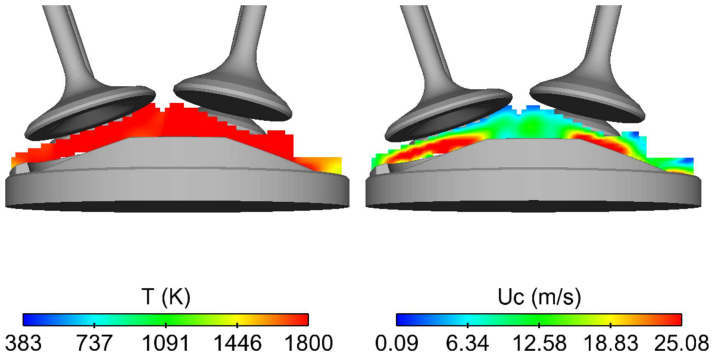

FIGURE 11. Reactive case at 733 CAD. left: temperature; right: velocity.

Ingnition (SACI) is shown to help stabilizing the transition. Since the combustion regimes involved in HCCI and SI case are different, some model development concerning the SACI regime is necessary in order to understand the physics of the transition.

Acknowledgments

Support from the Robert Bosch Corporation is gratefully acknowledge. Moreover, the authors would like to thank Eric Doran and Dave Cook from the Robert Bosch Corporation for a fruitful collaboration.

REFERENCES

BARTHS, H., PITSCH, H. & PETERS, N. 1999 3d simulation of DI diesel combustion and pollutant formation using a two-component reference fuel. *Oil & Gas Science & Technology* **54** (2), 233–244.

BAUMGARTEN, C. 2006 *Mixture formation in internal combustion engines*. Springer Berlin, Germany.

DE CHAISEMARTIN, S. 2009 Eulerian models and numerical simulation of turbulent dispersion for polydisperse evaporation sprays. PhD thesis, Ecole Centrale Paris, France, available on TEL : http://tel.archives-ouvertes.fr/tel-00443982/en/.

Dillon, H. & Penoncello, S. 2004 A fundamental equation for calculation of the thermodynamic properties of ethanol. *Int. J. Thermophysics* **25** (2), 321–335.

Donea, J., Huerta, A., Ponthot, J.-P. & Rodriguez-Ferran, A. 2004 Arbitrary Lagrangian-Eulerian methods. *Enc. Comp. Mec.* pp. 413–437.

Doran, E. 2011 A multi-dimensional flamelet model for ignition in multi-feed combustion systems. PhD thesis, Stanford University.

Dumouchel, C. 2009 The maximum entropy formalism and the prediction of liquid spray drop-size distribution. *Entropy* **11** (4), 713–747.

Germano, M., Piomelli, U., Moin, P. & Cabot, W. 1991 A dynamic subgrid-scale eddy viscosity model. *Phys. Fluids A: Fluid Dynamics* **3**, 1760.

http://webbook.nist.gov/chemistry/ 2011 *NIST Chemistry WebBook, NIST Standard Reference Database*. Linstrom, P. J. and Mallard, W. G.

Kah, D. 2010 Taking into account polydispersity for the modeling of liquid fuel injection in internal combustion engines. PhD thesis, Ecole Centrale Paris.

Meneveau, C. & Katz, J. 2000 Scale-invariance and turbulence models for large-eddy simulation. *Ann. Rev. of Fluid Mech.* **32** (1), 1–32.

Meneveau, C., Lund, T. & Cabot, W. 1996 A Lagrangian dynamic subgrid-scale model of turbulence. *J. Fluid Mech.* **319** (1), 353–385.

Miller, R. S. & Bellan, J. 1999 Direct numerical simulation of a confined three-dimensional gas mixing layer with one evaporating hydrocarbon-droplet-laden stream. *J. Fluids Mech.* **384**, 293–338.

Mittal, V. 2012 A multi-regime combustion model for reactive flow in internal combustion engines. PhD thesis, Stanford University.

Mittal, V., Cook, D. & Pitsch, H. 2012 An extended multi-regime flamelet model for ic engines. *Comb. Flame* .

Muller, B. 1998 Low Mach number asymptotics of the Navier-Stockes equations. *Journal of Engineering Mathematics* **34** (97-109).

O'Rourke, P. J. 1981 Collective drop effects on vaporizing liquid sprays. PhD thesis, Princeton University.

Peters, N. 1984 Laminar diffusion flamelet models in non-premixed turbulent combustion. *Progress in Energy and Combustion Science* **10** (3), 319–339.

Pitsch, H., Barths, H. & Peters, N. 1996 Three-dimensional modeling of NOx and soot formation in DI-diesel engines using detailed chemistry based on the interactive flamelet approach. *SAE paper* **962057**.

Poinsot, T. & Veynante, D. 2005 *Theoretical and Numerical Combustion*, 2nd edn. Philadelphia: Edwards.

Sazhin, S. 2006 Advanced models of fuel droplet heating and evaporation. *Progress in Energy and Combustion Science* **32** (2), 162–214.

Shashank, Knudsen, E. & Pitsch, H. 2011 Spray evaporation model sensitivities. *Annual Research Brief, Stanford University* .

Smagorinsky, J. 1963 General circulation experiments with the primitive equations. *Monthly weather review* **91** (3), 99–164.

Stanescu, D. & Habashi, W. 1998 2 N-storage low dissipation and dispersion runge-kutta schemes for computational acoustics. *Journal of Computational Physics* **143** (2), 674–681.